An expanded sequence context model broadly explains variability in polymorphism levels across the human genome

Varun Aggarwala[1] & Benjamin F Voight[2,3]

The rate of single-nucleotide polymorphism varies substantially across the human genome and fundamentally influences evolution and incidence of genetic disease. Previous studies have only considered the immediately flanking nucleotides around a polymorphic site—the site's trinucleotide sequence context—to study polymorphism levels across the genome. Moreover, the impact of larger sequence contexts has not been fully clarified, even though context substantially influences rates of polymorphism. Using a new statistical framework and data from the 1000 Genomes Project, we demonstrate that a heptanucleotide context explains >81% of variability in substitution probabilities, highlighting new mutation-promoting motifs at ApT dinucleotide, CAAT and TACG sequences. Our approach also identifies previously undocumented variability in C-to-T substitutions at CpG sites, which is not immediately explained by differential methylation intensity. Using our model, we present informative substitution intolerance scores for genes and a new intolerance score for amino acids, and we demonstrate clinical use of the model in neuropsychiatric diseases.

Measured at the level of the chromosome down to individual base, rates of single-nucleotide substitution vary substantially by position across mammalian genomes, including in humans[1]. An exquisite example of the role for sequence context in contributing variability in substitution rate is provided by CpG dinucleotides, where spontaneous deamination of 5-methylcytosine results in ~14-fold higher C-to-T substitution rates as compared to the genome-wide average[1–3]. Modeling the variability in nucleotide substitution rates will inform understanding of evolutionary processes, help identify functional noncoding regions[4] and mutation-promoting motifs, suggest mechanisms behind spontaneous mutation and aid in prediction of the clinical impact of polymorphisms discovered through resequencing[5]. Such models will need to determine not only the optimal window of local sequence context but should also integrate knowledge of functional constraint on the genome due to pressure from purifying selection.

Studies of complex human disease have incorporated a simple trinucleotide sequence context[6,7] into models to quantify the probability of *de novo* mutational events[8–10], to clarify the distribution of somatic mutational events segregating in different cancers[11] and to model the purifying selective pressure on gene sequences[12]. As their focus was clinical, these reports did not determine whether this context model best captured the extent to which flanking nucleotides influence the variability in genome-wide nucleotide substitution rates. Here we report a statistical framework that compares the extent to which different local sequence lengths influence the probability of nucleotide substitution, tested using data from the 1000 Genomes Project[13]; apply our models to the coding genome; and demonstrate use of the model to interpret *de novo* mutations identified in studies of neuropsychiatric disorders. We define the probability of nucleotide substitution as the chance that a nucleotide in the human genome reference is polymorphic, that is, the nucleotide position segregates alternative nucleotides within the population. This probability depends on population history, selection, sample ascertainment and local context features that influence the rate of mutation.

RESULTS

Sequence context modeling of substitution probabilities

We hypothesized that local sequence context—the nucleotides that flank a polymorphic site—could explain the observed variability in nucleotide substitution probabilities. To test this hypothesis, we defined a statistical model (Online Methods and **Supplementary Fig. 1**) whereby the probability that a nucleotide substitution occurs at a genomic site varies according to (i) the identities of the nucleotides that flank the site and (ii) the size of the 5′-to-3′ local sequence context window. To minimize the impact of natural selection, we focused on intergenic noncoding regions of the genome (Online Methods). As the estimated nucleotide substitution probabilities were robust (**Supplementary Table 1a**), we developed a likelihood-ratio testing procedure to evaluate competing local sequence context models (Online Methods).

First, we calculated the likelihood of the observed data assuming a '1-mer' model, which allowed different substitution classes (for example, A to G, C to T, etc.) to occur at different rates but ignored the effects of sequence context on substitution probabilities. We compared the 1-mer model to the trinucleotide ('3-mer') sequence context model where single 5′ and 3′ nucleotides flanking the polymorphic middle position influence the rate of substitution. As expected, the 3-mer model significantly improved fit to the data (log-likelihood ratio (LLR) = 6,070,948, $P << 1 \times 10^{-100}$; **Supplementary Table 1a**).

[1]Genomics and Computational Biology Program, Perelman School of Medicine, University of Pennsylvania, Philadelphia, Pennsylvania, USA. [2]Department of Systems Pharmacology and Translational Therapeutics, Perelman School of Medicine, University of Pennsylvania, Philadelphia, Pennsylvania, USA. [3]Department of Genetics, Perelman School of Medicine, University of Pennsylvania, Philadelphia, Pennsylvania, USA. Correspondence should be addressed to B.F.V. (bvoight@upenn.edu).

Received 14 April 2015; accepted 22 January 2016; published online 15 February 2016; doi:10.1038/ng.3511

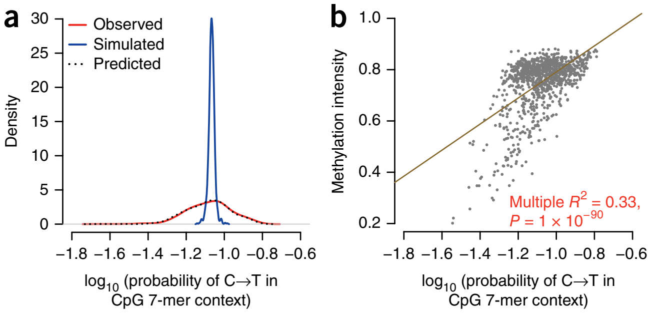

Figure 1 C-to-T substitution probabilities and methylation patterns in 7-mer CpG sequence contexts. (**a**) Simulations based on a fixed C-to-T substitution rate (blue) in CpG contexts do not capture the observed distribution of substitution probabilities (red) in the 7-mer sequence context. Rates predicted from our regression model (black) closely match the substitution probabilities observed under the 7-mer sequence context ($R^2 = 0.93$). (**b**) Correlation between average methylation intensity and probability of C-to-T substitution in the CpG 7-mer context.

Next, we evaluated whether the inclusion of additional local nucleotides could further improve fit to the observed data. We demonstrate that, when compared to the 3-mer model or the pentanucleotide ('5-mer') model (with two flanking nucleotides on each side), the larger, heptanucleotide ('7-mer') model (with three flanking nucleotides on each side) fit the data better (both LLR >494,212, $P << 1 \times 10^{-100}$; **Supplementary Table 1b**). To further validate the models, we estimated substitution probabilities using 1,659,929 HapMap[14] variants found in our noncoding regions (Online Methods) and observed that 7-mer context probabilities strongly correlated with probabilities estimated from 1000 Genomes Project data (**Supplementary Fig. 2** and **Supplementary Table 2**) and provided the best fit to the observed polymorphisms (**Supplementary Table 3**). Our model recapitulates expected shifts in probabilities consistent with population histories[15] (**Supplementary Fig. 3**) and the downward shift in the average substitution probability for the X chromosome[16] relative to the autosomes (**Supplementary Table 4**) due to the smaller effective population size at the X chromosome. Taken collectively, our analyses demonstrate for the first time, to our knowledge, that a 7-mer sequence context model explains the observed distribution of polymorphisms found in human populations.

To incorporate prior information, we developed a Bayesian formulation using objective conjugate priors for analysis of the noncoding genome (Online Methods). Consistent with our previous analysis, the 7-mer context model proved superior in comparison to all other models (approximate Bayes factor (ABF) >> 1,000; **Supplementary Table 1c**). In subsequent analyses, we use these posteriors for the nucleotide substitution probabilities.

7-mer context predicts noncoding substitution rates

To quantify the variance in the posterior probabilities that a 7-mer sequence context model could explain, we considered each substitution class separately, as well as CpG site contexts (nine classes in total). We employed forward regression (Online Methods) to select features from a 7-mer context window to predict substitution probabilities and considered up to four-way interactions at positions within the window. When compared to single-base and position models without interactions, incorporating higher-order interactions substantially improved the fit to data (**Supplementary Table 5**). Specifically, we found that our selected models in a separately held test data set explained a median of 81% of the variability (as compared to 30% explained by the 3-mer context) in probabilities across all substitution classes, covering 84% of all mutational events and fitting well the probability of C-to-T substitution at CpGs (**Fig. 1a** and **Table 1**). Although we identified a common set of interactions across classes (**Supplementary Table 6**), many common features did not always influence substitution probabilities in the same way and others had class-specific effects. These observations indicate that core and class-specific features based on sequence context are predictive of the potential for nucleotide substitution.

Methylation cannot fully explain patterns at CpG sites

The spontaneous deamination of 5-methylcytosine at CpG sites results in ~14-fold higher rates of C-to-T substitutions generally[3,17]. Although a previous report indicated that divergence at CpG sites varies as a function of local context, the focus was on introns and did not consider population-level polymorphisms in humans[18]. Thus, we hypothesized that the surrounding sequence context further influences the probability of nucleotide substitution at CpGs and examined the C-to-T substitution class within the subset of contexts that contained a CpG at positions 4 and 5 in the 7-mer. Simulations using a model that ignored additional genomic context, or considered the 3-mer context (**Supplementary Fig. 4**), using a fixed CpG substitution probability generated significantly less variability in 7-mer CpG substitution probabilities than was empirically observed (empirical $P << 1 \times 10^{-10}$; **Fig. 1a**). These data indicate that (i) not all CpG sites accrue substitutions at the same rate and (ii) the sequence context surrounding CpG sites correlates with biological features or mechanisms that influence this rate.

To explore the possibility that the excess variability depends on variation in methylation intensity across sequence contexts, we reanalyzed whole-genome bisulfite sequencing data obtained from germline and other tissues of healthy individuals[19,20]. Comparing the CpG sites that are consistently methylated with those that are consistently unmethylated across subjects, we observed as expected that methylation correlates with an increase in the probability of C-to-T substitution ($P << 1 \times 10^{-100}$; **Supplementary Fig. 5**). Unexpectedly, when we compared the methylation intensity in sperm at 7-mer CpG contexts with the probability of substitutions, we found a positive but imperfect correlation ($R^2 = 0.33$, $P < 1 \times 10^{-90}$; **Fig. 1b**), with similar results in other tissues (**Supplementary Fig. 6**), noting instances of methylation status decoupled from substitution probabilities. For example, nearly every genomic instance of the sequence contexts

Table 1 Summary and performance of forward regression model for feature selection using the 7-mer context in the intergenic noncoding genome

Substitution class	Contexts (n)	Substitutions (%)[a]	Parameters (n)[b]	Model R^2 (7-mer)[c]	Model R^2 (3-mer)[d]
Outside CpG dinucleotide context					
A to C	4,096	7.3	266	56.5	11.2
A to G	4,096	28.2	366	91.5	40.9
A to T	4,096	7.1	197	58.7	37.4
C to A	3,072	8.5	282	83.5	30.0
C to G	3,072	7.5	268	81.0	17.1
C to T	3,072	24.4	254	86.8	37.6
Within CpG dinucleotide context					
C to A	1,024	1.0	26	58.3	19.0
C to G	1,024	0.8	95	48.7	9.5
C to T	1,024	15.2	96	93.1	44.4

[a] The percentage of substitutions for that class observed in the genome. [b] The number of features selected in the best 7-mer model. [c] Prediction accuracy in the test data set alone (not used for model training) with the best model using the 7-mer sequence context features. [d] Prediction accuracy with only the 3-mer sequence context features.

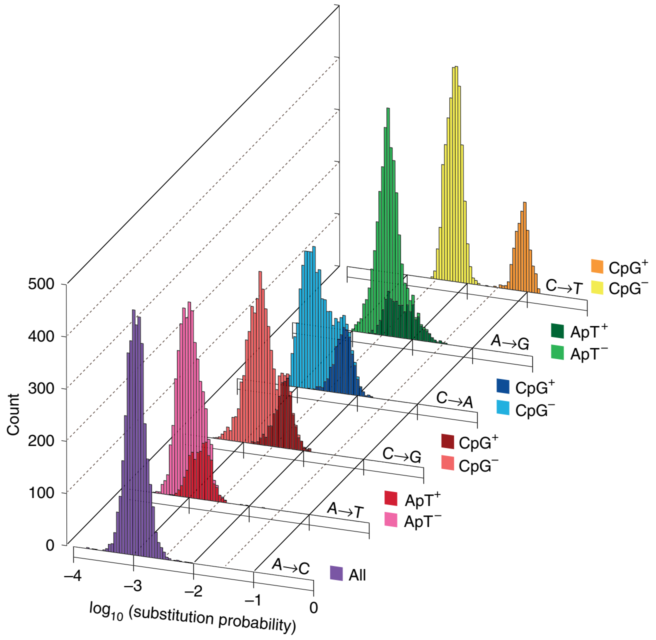

Figure 2 Posterior probabilities of all classes of nucleotide substitution in the intergenic noncoding genome, estimated using the 7-mer context model. Sequence contexts are further stratified by color to indicate either CpG status (C at the polymorphic position 4 and G at position 5, for C-to-A, C-to-G and C-to-T substitution classes, CpG$^+$; otherwise, CpG$^-$) or ApT status (A at the polymorphic position 4 and T at position 5, for A-to-G and A-to-T substitution classes, ApT$^+$; otherwise, ApT$^-$). For A-to-C substitutions, ApT status did not significantly contribute to variability in the estimated probability distribution.

GTACGCA and GATCGCA showed consistent methylation signals (both methylated in >94% of occurrences in sperm); the probability of C-to-T transition was more than twofold different for these two contexts (0.148 versus 0.07, respectively). These data are consistent with the hypothesis that local context features beyond DNA methylation influence probabilities of C-to-T transitions at CpG sites, although we cannot exclude the possibility that subtissue methylation differences could explain these patterns.

Identification of new mutation-promoting motifs

We next investigated the substitution probabilities for 7-mer contexts partitioned by substitution class (**Fig. 2** and **Supplementary Table 7**). First, we noted that several classes (C-to-A and C-to-G in addition to C-to-T changes) appeared to segregate as mixtures of two distributions, explainable by CpG effects. These observations are consistent with studies demonstrating elevated rates of substitution at CpGs in humans[21], although this early work was not powered to measure context dependencies surrounding CpG sites as we are here. As the methylation transition state intermediate 5-formylcytosine can induce spontaneous C-to-A or C-to-G substitutions[22], one possibility is that methylation also elevates these rates in this context. We next determined whether local sequence context motifs—analogous to but beyond CpG dinucleotides—correlate with variable substitution probabilities across classes (Online Methods). We noted that poly(CG) sequences in the lower tail of C-to-T substitutions for the CpG context were enriched ($P < 1 \times 10^{-16}$; **Table 2**). This observation is consistent with previous reports[23], as this context is found proximal to genes (**Supplementary Fig. 7**) and is associated with lower methylation intensities (**Supplementary Fig. 8**). In the upper tail of the A-to-T substitution class, we observed a poly(T) + poly(A) motif in the outlier sequences ($P < 1 \times 10^{-5}$; **Table 2**). We also observed a similar A_4 motif in the lower tail of the A-to-G class ($P < 1 \times 10^{-10}$). One possible mechanism that might contribute is the 'slippage' of protein machinery during DNA replication[24]. Our analysis also identified motifs without an obvious contributing mechanism. First, in the upper tail of CpG rates, we observed enrichment of a TACG motif ($P < 1 \times 10^{-10}$; **Table 2**) that was strongly methylated (**Supplementary Fig. 8**), but, curiously, a similar motif shifted by one position was enriched in the lower tail of the A-to-C class ($P < 1 \times 10^{-4}$). Second, the ApT dinucleotide was found to elevate the substitution probabilities (**Fig. 2**) for the A-to-G ($P < 1 \times 10^{-25}$) and A-to-T ($P < 1 \times 10^{-17}$) classes, although not statistically significantly so for the A-to-C class. Finally, we observed a CAAT motif also enriched in the upper tail of the A-to-G substitution class ($P < 1 \times 10^{-53}$), reported in an earlier study of dbSNP variants[25]. These latter cases indicate potentially new mechanisms contributing to elevated nucleotide substitutability, not documented by the commonly used trinucleotide context model. As a final analysis of robustness, keeping in mind limitations due to variant ascertainment, we estimated the substitution probabilities using HapMap variants and found similar mutation-promoting motifs across substitution classes (**Supplementary Table 8**).

Experiments to validate the noncoding rate model

If the estimated noncoding substitution probabilities reflect properties of mutation, one would expect that these rates should (i) not be influenced by rates of recombination, (ii) strongly correlate with rates of species divergence[26], (iii) be consistent for both rare and common genetic variants, and (iv) also be reflected in *de novo* mutational events. We explored each of these predictions in turn. First, we estimated the 7-mer substitution rates from all intergenic noncoding variants separately for regions with high and low recombination rates and found a strong correlation between the two ($R^2 = 0.97$, $P < < 1 \times 10^{-100}$; Online Methods and **Supplementary Fig. 9**), indicating that substitution probabilities estimated from the noncoding genome are correlated across high and low rates of recombination. Next, using human-chimpanzee and human-macaque alignments over intergenic noncoding sequences, we found a strong correlation between divergence and substitution probabilities for our 7-mer contexts (both $R^2 = 0.96$, $P < < 1 \times 10^{-100}$; Online Methods, **Supplementary Fig. 10** and **Supplementary Table 9**). We then estimated 7-mer probabilities from all intergenic noncoding rare variants (singletons and doubletons) separately from low- and high-frequency (>1%) variants and found a strong correlation ($R^2 = 0.98$, $P < < 1 \times 10^{-100}$; Online Methods and **Supplementary Fig. 11**), as well as a superior 7-mer context fit to data across variant frequencies (**Supplementary Table 10**). Finally, we obtained 4,748 *de novo* mutational events from a high-quality pedigree sequencing data set on 78 parent-offspring trios[27]. We tested for the presence of the motifs we identified in **Table 2** around *de novo* events and observed a significant enrichment (Online Methods and **Supplementary Table 11**). Taken collectively, these findings provide additional validation for the hypothesis that our substitution probabilities capture features of germline mutation.

7-mer context also predicts exonic substitution rates

Assuming that the processes that generate spontaneous mutations apply uniformly across the genome, we hypothesized that sequence context could explain variability in substitution probabilities in the coding genome. We therefore extended our initial framework (Online Methods and **Supplementary Fig. 1**) to the coding genome

Table 2 Enrichment of motifs identified in posterior nucleotide substitution probabilities for the 7-mer sequence context models inferred from the intergenic noncoding genome

Motif	Substitution class	Effect on substitution probability[b]	Enrichment *P* value	OR (95% CI)[c]	Fold change in substitution rate[d]
NNN$\underline{\text{C}}$GNN	C to T	Higher	2×10^{-26}	134.4 (18.4–977.4)	13.9
	C to G	Higher	1×10^{-13}	12.8 (5.9–27.7)	2.4
	C to A	Higher	9×10^{-22}	60.8 (14.6–252.1)	2.7
N[A/C/G][C/G/T]$\underline{\text{C}}$GCG	C to T (CpG+)[a]	Lower	7×10^{-16}	366.3 (45.6–2,939.5)	1.5
Poly(T) and poly(A) combination (AAA$\underline{\text{A}}$TTT, TTT$\underline{\text{A}}$AAA)	A to T	Higher	9×10^{-5}	304.2 (31.0–2,987.6)	12.7
A_4 (AAA$\underline{\text{A}}$NNN, NAA$\underline{\text{A}}$ANN, NNA$\underline{\text{A}}$AAN, NNN$\underline{\text{A}}$AAA)	A to G	Lower	5×10^{-10}	10.2 (7.3–14.1)	1.9
NTA$\underline{\text{C}}$G[C/G][A/C/G]	C to T (CpG+)[a]	Higher	1×10^{-10}	102.5 (27.4–383.2)	1.7
NNT$\underline{\text{A}}$CGN	A to C	Lower	3×10^{-4}	9.4 (3.6–24.8)	1.5
NNN$\underline{\text{A}}$TNN	A to T	Higher	2×10^{-17}	22.3 (8.7–57.1)	1.6
	A to G	Higher	1×10^{-25}	131.2 (18.0–954.2)	2.0
[C/T]CA$\underline{\text{A}}$T[C/G/T]N	A to G	Higher	8×10^{-53}	5,966 (2,091–17,021)	5.1

In the motifs, the polymorphic nucleotide is underlined.
[a] The distribution of sequence contexts that include a CpG site (where the polymorphic site at position 4 is C and position 5 is fixed as G). [b] Based on the enrichment of the motif in the 1% tail of the given substitution class: "Higher" implies enrichment in the upper 1% tail of the sequence context probability distribution, and "Lower" implies enrichment in the lower 1% tail of this distribution. [c] The odds ratio (and 95% confidence interval) of enrichment of the motif in the upper or lower 1% tail of the sequence context probability distribution. [d] The fold increase or decrease in substitution rates for the motif relative to its substitution class.

by (i) using information obtained from our model on the noncoding genome as the prior and (ii) allowing for context dependence of codons and local sequence context in our estimates of substitution probabilities to accommodate purifying selective pressure[28]. Our new model substantially improved the fit to the data as compared to the 3-mer sequence context models with or without codon context (ABF >> 1,000; **Supplementary Table 12**). To further validate, we tested our model on a different large-scale exome sequencing data set from ~4,300 individuals[29] and noted that our 7-mer model fit patterns of exonic polymorphisms better than competing models (ABF >> 1,000; Online Methods and **Supplementary Table 12**). These results demonstrate, for the first time to our knowledge, that a broader sequence context—beyond simple codon or trinucleotide context—captures the forces that shape variability in nucleotide substitutions in the coding genome.

We then examined the posterior distribution of substitution probabilities for all contexts stratified by the type of amino acid substitution (**Supplementary Fig. 12** and **Supplementary Table 13**) and found excess variability in each class over that expected under simulation (Online Methods and **Supplementary Table 14**). Next, we enumerated the substitution probability profiles for each amino acid change and found certain nonsense and missense substitution probabilities to be higher than synonymous levels (**Supplementary Fig. 13**), partially explained by CpG contexts. These observations caution against the practice—invoked in rare variant association tests—of ignoring codon and sequence context when testing for the burden of functional substitutions. Our results here demonstrate that functional substitutions may not be equally likely or tolerated with respect to purifying selection.

7-mer context improves power to detect pathogenic variants

We now turn to applications of our model to improve the interpretation of variation discovered by clinical resequencing. Efforts to prioritize variants from such studies often rely on classifying variants that are deleterious with respect to population genetic fitness, hypothesizing that such variants are more likely to be pathogenic[30]. As our coding substitution probabilities are influenced by forces both of mutation (estimated from the noncoding genome) and selection, we hypothesized that the ratio of these probabilities quantifies the action of selective pressure and could be used to prioritize pathogenic variants. To test this hypothesis, we calculated the log ratio of intergenic noncoding and coding substitution probabilities, defined as the sequence constraint score, for missense ($n = 48{,}450$) and nonsense ($n = 12{,}054$) variants present in the Human Gene Mutation Database (HGMD; Online Methods)[31]. We observed that the distribution of sequence constraint scores for HGMD variants was shifted toward larger values (intolerance) as compared to 1000 Genomes Project variants ($P < < 1 \times 10^{-100}$; **Fig. 3a**), compatible with the 'intolerant variant, pathogenic variant' hypothesis. Moreover, the distribution of scores based on our 7-mer model was further shifted toward intolerance with a thicker tail, as compared to a 3-mer model ($P < < 1 \times 10^{-100}$; **Supplementary Fig. 14**). These data demonstrate that a coding model

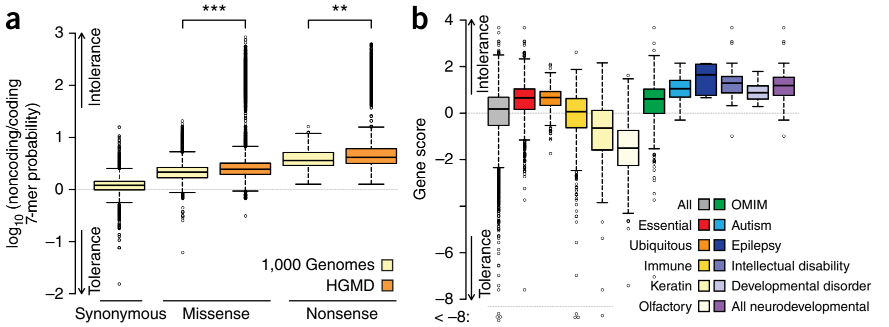

Figure 3 Prioritizing pathogenic variants and causal genes using constraint scores. (**a**) Log_{10} ratios of substitution probabilities from the 7-mer sequence context model using coding sequences matched to intergenic noncoding sequences, for each type of substitution (synonymous, missense and nonsense) for all variants in the 1000 Genomes Project or HGMD. Larger values indicate fewer substitutions in the coding genome than expected from matched noncoding sequences, consistent with the action of selective constraint. $^{***}P < < 1 \times 10^{-100}$, $^{**}P < 1 \times 10^{-29}$. (**b**) Box-and-whisker plots of gene scores from the model, stratified into statistically significant gene classes. Positive gene scores indicate intolerance to substitutions that change an amino acid. For the box plots, the center line in each box denotes the median. The interquartile range (25th to 75th percentile) is indicated by the ends of each box. The whiskers extend to 1.5 times the interquartile range, and data points beyond this range are plotted as open circles.

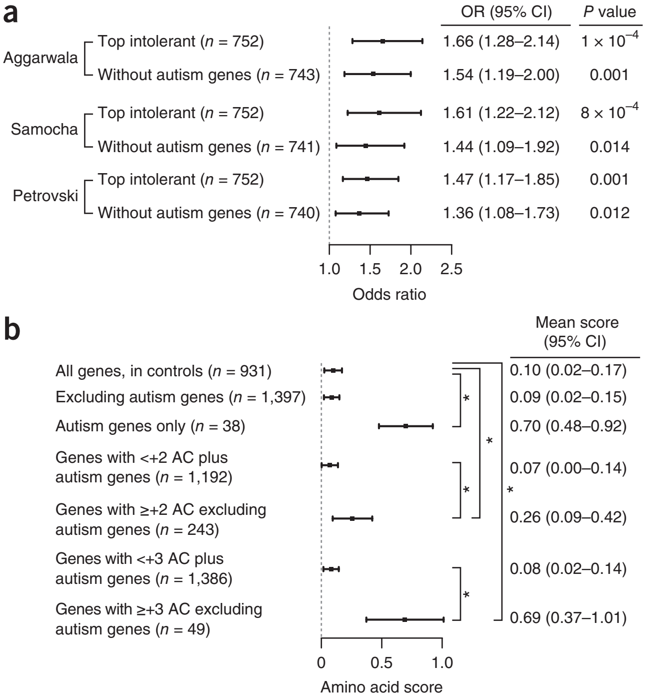

Figure 4 Application of gene and amino acid intolerance scores to *de novo* autism spectrum disorder mutational data. (**a**) Forest plots of the odds ratios (ORs), 95% confidence intervals (CIs) and *P* values when comparing the *de novo* mutational burden in cases and controls on intolerant genes identified using different gene scoring methods. Scores were calculated including and excluding known autism-associated genes, as indicated. Aggarwala indicates gene scores from this report, and Samocha and Petrovski refer to the intolerant gene lists from refs. 12,32. (**b**) Forest plots of the mean amino acid scores with 95% confidence intervals found from *de novo* mutations in various gene collections. Average scores were based on variants ascertained in cases, except where noted (the first row corresponds to all genes in controls). +AC, excess count of missense or nonsense changes in cases relative to controls. For example, +3 indicates that a gene has three more missense or nonsense changes in cases relative to controls. $^*P < 0.01$.

that includes the codon and 7-mer context improves the identification of variants that are potentially pathogenic.

Describing genic intolerance to mutation via 7-mer context

Several groups have argued that the power to identify causal disease genes from clinical resequencing data could be enhanced by incorporating estimates of selective constraint on genes[12,32,33]. The underlying hypothesis behind this concept is that genes that are under selective constraint are more likely to show functional consequences when altered and are therefore most likely to be pathogenic and have fewer functional variants ('intolerant gene, pathogenic gene'). The community has successfully applied this concept to neurodevelopmental and psychiatric disorders[34]; however, the existing approaches have not incorporated the 7-mer sequence or codon context in their models.

Therefore, we applied our 7-mer coding substitution probabilities to develop an intolerance score (Online Methods and **Supplementary Table 15**) quantifying the difference between the expected and observed numbers of functional variants at a gene, with higher scores consistent with functional constraint. To further validate, we found gene scores on a separate, larger exome sequencing data set and observed a strong correlation between the two (**Supplementary Fig. 15**). We found that genes belonging to putatively essential or ubiquitously expressed categories scored strongly for genic intolerance ($P << 1 \times 10^{-100}$; **Fig. 3b**). In contrast, gene sets representing keratin and olfactory categories were found to be highly tolerant of functional changes (**Fig. 3b**). Next, we applied this to Online Mendelian Inheritance in Man (OMIM) genes or the known genes behind several neuropsychiatric disorders such as autism[35], epilepsy[36], developmental disorder[37] and intellectual disability[38–40] and found these genes to have significantly higher intolerance scores ($P << 1 \times 10^{-100}$; **Fig. 3b**). We then compared our gene scores to previously reported scores (Online Methods and **Supplementary Fig. 16**) and found that our approach improved classification or performed comparably to other approaches[32] for genes in each set, including the disease categories (**Supplementary Table 16**). These results demonstrate that the most accurate scoring of genic tolerance to functional substitution can be achieved by modeling 7-mer sequence and coding context.

An amino acid score for pathogenic variant prioritization

Beyond the average rate of amino acid replacement that a gene might tolerate, genes could be further intolerant to specific types of amino acid substitutions, signifying added localized selective constraint or importance for gene functionality. Therefore, we developed a score measuring the intolerance at the level of amino acid replacement for a gene (Online Methods and **Supplementary Table 17**), after quantifying the difference between the expected and observed numbers of functional variants for a specific amino acid at a gene. Across all genes represented in HGMD with a large number of putatively pathogenic amino acid changes for a specific substitution, we found that these genes segregate larger intolerance scores for that amino acid (empirical $P < 1 \times 10^{-10}$). Moreover, a gene might score 'tolerant' for functional substitution but 'intolerant' for specific amino acid changes. For example, *VWF* (encoding von Willebrand factor), a blood glycoprotein involved in hemostasis, is tolerant to substitution overall (within the top 8% of gene tolerance) but intolerant to cysteine substitution (within the top 3.5% of cysteine intolerance). These data are consistent with a causal mechanism for von Willebrand disease: protein misfolding when cysteine residues are substituted[41]. We note that 5,652 genes segregate a profile similar to that of *VWF*, showing average genic tolerance but amino acid intolerance.

Interpretation of *de novo* mutations discovered in autism

Autism spectrum disorder is a disease with complex etiology, and recent efforts have aimed to identify *de novo* mutational events that may contribute to disease. To highlight the usefulness of gene[12,32] and amino acid scores, we applied them to interpret the *de novo* mutations collected from 2,508 autism spectrum disorder[42] cases and 1,911 control family trios. First, we found that the most intolerant genes based on our gene score segregated a significant burden of *de novo* mutations in cases as opposed to controls (odds ratio (OR) = 1.66, $P < 0.0001$; **Fig. 4a** and Online Methods), even after removing known autism-associated genes[35] (OR = 1.54, $P < 0.001$), and similar although slightly attenuated burden using other scores (**Fig. 4a**). Next, we found that the average amino acid score for *de novo* mutations at autism-associated genes in cases was higher (more intolerant) than that found in controls or at other genes in cases ($P = 0.002$; **Fig. 4b** and Online Methods). We further observed higher (intolerant) average amino acid scores for variants in genes with a positive variant burden in cases relative to controls (+2 or +3 allele count excess in cases; both $P < 0.01$; **Fig. 4b**). Finally, several genes from the excess allele count set stood out with amino acid–specific intolerance (all within the top four percentiles of intolerance): *MYO9B*, *WDFY3*, *NAV2*, *STIL* and *SCUBE2*. Aside from *WDFY3*, these genes are generally tolerant, on the basis of their gene score, indicating the usefulness of subgene-wise measurement of functional intolerance. While *MYO9B* has been implicated in autism[35] and *Wdfy3* deletions in a mouse model have been shown to cause autism-like symptoms[43], our analysis points to the remaining candidates for future follow-up.

DISCUSSION

We report a sequence context model that explains patterns of nucleotide substitution observed in the human genome. Our motivation was based on the need to statistically evaluate competing models for sequence context. We demonstrate that the commonly used context that includes one nucleotide flanking each side of a polymorphic site does not fully capture the complete spectrum of where, what type and how frequently nucleotides are expected to change. Furthermore, by using population-level data rather than data on *de novo* or somatic events, we were able to improve the resolution of substitution models and identify new mutation-promoting motifs. Our approach also characterized average selective pressures operating in the coding genome at a finer level of detail. Our model indicates substantial variability across all amino acid replacement classes and, in some cases, synonymous substitutions that were less prone to change than missense or even nonsense substitutions. We suggest that inference of the presence and strength of selection on genes might further benefit from incorporating information at this resolution.

One question in the field has been how much sequence context can explain patterns of nucleotide substitution in genomes[44]. Our results suggest that a substantial fraction of variability can be robustly predicted by sequence context alone, although specific substitution classes may require more than sequence context for their prediction. In evolutionary genetics studies, the set of substitutions that occurs at nearly constant rates proportional to the lineage (the most ‘clock-like’) is important for accurate dating of divergence events[45]. Although we did not apply our model to other species, the strong correlation with divergence suggests that our features are potentially conserved across primates.

We acknowledge that a number of features remain to be formally evaluated in the genome[46], for example, recombination in the coding genome[47] or replication timing[48]. Our framework has the flexibility to model the complexity found in any sequences that contain features hypothesized to be important. We also acknowledge that context models including more than three flanking nucleotides on each side of a polymorphism were not considered. The regression approach we have presented does suggest that the 7-mer models could be refined, perhaps allowing a broader context to be considered.

With an appropriate background model for nucleotide substitution, new statistics for clinical resequencing studies can be envisioned, based on the occurrence of discovered variation. Such approaches may complement statistics that assay allele frequency differences between cases and controls at one or more polymorphic sites. Moreover, comparative genomics applications to identify non-neutrally evolving regions, genome alignments or tree reconstruction[49] would benefit from accurate models of nucleotide substitution. Although the underlying mechanisms that determine how nucleotide sequences change over time remain to be addressed, we posit that the features identified from our model provide important clues in elucidating these fundamental principles.

URLs. Exome Variant Server (EVS), http://evs.gs.washington.edu/EVS/.

METHODS

Methods and any associated references are available in the online version of the paper.

Note: Any Supplementary Information and Source Data files are available in the online version of the paper.

ACKNOWLEDGMENTS

We thank C. Brown, M. Bucan, P. Babb, K. Siewert, K. Johnson, S. Bumgarner and two anonymous reviewers for helpful comments on the manuscript. B.F.V. is grateful for support of the work from the Alfred P. Sloan Foundation (BR2012-087), the American Heart Association (13SDG14330006), the W.W. Smith Charitable Trust (H1201) and the US National Institutes of Health/National Institute of Diabetes and Digestive and Kidney Disorders (R01DK101478).

AUTHOR CONTRIBUTIONS

V.A. and B.F.V. conceived and designed the experiments, developed the model, performed the statistical analysis, developed and contributed analysis tools, and wrote the manuscript. B.F.V. supervised the research.

COMPETING FINANCIAL INTERESTS

The authors declare no competing financial interests.

1. Hodgkinson, A. & Eyre-Walker, A. Variation in the mutation rate across mammalian genomes. *Nat. Rev. Genet.* **12**, 756–766 (2011).
2. Ehrlich, M. & Wang, R.Y. 5-methylcytosine in eukaryotic DNA. *Science* **212**, 1350–1357 (1981).
3. Rideout, W.M. III, Coetzee, G.A., Olumi, A.F. & Jones, P.A. 5-methylcytosine as an endogenous mutagen in the human LDL receptor and p53 genes. *Science* **249**, 1288–1290 (1990).
4. Arbiza, L. *et al.* Genome-wide inference of natural selection on human transcription factor binding sites. *Nat. Genet.* **45**, 723–729 (2013).
5. Yang, Y. *et al.* Clinical whole-exome sequencing for the diagnosis of mendelian disorders. *N. Engl. J. Med.* **369**, 1502–1511 (2013).
6. Hwang, D.G. & Green, P. Bayesian Markov chain Monte Carlo sequence analysis reveals varying neutral substitution patterns in mammalian evolution. *Proc. Natl. Acad. Sci. USA* **101**, 13994–14001 (2004).
7. Blake, R.D., Hess, S.T. & Nicholson-Tuell, J. The influence of nearest neighbors on the rate and pattern of spontaneous point mutations. *J. Mol. Evol.* **34**, 189–200 (1992).
8. Neale, B.M. *et al.* Patterns and rates of exonic *de novo* mutations in autism spectrum disorders. *Nature* **485**, 242–245 (2012).
9. Michaelson, J.J. *et al.* Whole-genome sequencing in autism identifies hot spots for *de novo* germline mutation. *Cell* **151**, 1431–1442 (2012).
10. Fromer, M. *et al. De novo* mutations in schizophrenia implicate synaptic networks. *Nature* **506**, 179–184 (2014).
11. Lawrence, M.S. *et al.* Mutational heterogeneity in cancer and the search for new cancer-associated genes. *Nature* **499**, 214–218 (2013).
12. Samocha, K.E. *et al.* A framework for the interpretation of *de novo* mutation in human disease. *Nat. Genet.* **46**, 944–950 (2014).
13. 1000 Genomes Project Consortium. An integrated map of genetic variation from 1,092 human genomes. *Nature* **491**, 56–65 (2012).
14. International HapMap Consortium. A haplotype map of the human genome. *Nature* **437**, 1299–1320 (2005).
15. Campbell, M.C. & Tishkoff, S.A. African genetic diversity: implications for human demographic history, modern human origins, and complex disease mapping. *Annu. Rev. Genomics Hum. Genet.* **9**, 403–433 (2008).
16. Schaffner, S.F. The X chromosome in population genetics. *Nat. Rev. Genet.* **5**, 43–51 (2004).
17. Nachman, M.W. & Crowell, S.L. Estimate of the mutation rate per nucleotide in humans. *Genetics* **156**, 297–304 (2000).
18. Mugal, C.F. & Ellegren, H. Substitution rate variation at human CpG sites correlates with non-CpG divergence, methylation level and GC content. *Genome Biol.* **12**, R58 (2011).
19. Okae, H. *et al.* Genome-wide analysis of DNA methylation dynamics during early human development. *PLoS Genet.* **10**, e1004868 (2014).
20. Hovestadt, V. *et al.* Decoding the regulatory landscape of medulloblastoma using DNA methylation sequencing. *Nature* **510**, 537–541 (2014).
21. Walser, J.-C. & Furano, A.V. The mutational spectrum of non-CpG DNA varies with CpG content. *Genome Res.* **20**, 875–882 (2010).
22. Kamiya, H. *et al.* Mutagenicity of 5-formylcytosine, an oxidation product of 5-methylcytosine, in DNA in mammalian cells. *J. Biochem.* **132**, 551–555 (2002).
23. Deaton, A.M. & Bird, A. CpG islands and the regulation of transcription. *Genes Dev.* **25**, 1010–1022 (2011).
24. Levinson, G. & Gutman, G.A. Slipped-strand mispairing: a major mechanism for DNA sequence evolution. *Mol. Biol. Evol.* **4**, 203–221 (1987).
25. Panchin, A.Y., Mitrofanov, S.I., Alexeevski, A.V., Spirin, S.A. & Panchin, Y.V. New words in human mutagenesis. *BMC Bioinformatics* **12**, 268 (2011).
26. Lanfear, R., Welch, J.J. & Bromham, L. Watching the clock: studying variation in rates of molecular evolution between species. *Trends Ecol. Evol.* **25**, 495–503 (2010).
27. Kong, A. *et al.* Rate of *de novo* mutations and the importance of father’s age to disease risk. *Nature* **488**, 471–475 (2012).

28. Bustamante, C.D. *et al.* Natural selection on protein-coding genes in the human genome. *Nature* **437**, 1153–1157 (2005).
29. Fu, W. *et al.* Analysis of 6,515 exomes reveals the recent origin of most human protein-coding variants. *Nature* **493**, 216–220 (2013).
30. Cooper, G.M. & Shendure, J. Needles in stacks of needles: finding disease-causal variants in a wealth of genomic data. *Nat. Rev. Genet.* **12**, 628–640 (2011).
31. Stenson, P.D. *et al.* The Human Gene Mutation Database: building a comprehensive mutation repository for clinical and molecular genetics, diagnostic testing and personalized genomic medicine. *Hum. Genet.* **133**, 1–9 (2014).
32. Petrovski, S., Wang, Q., Heinzen, E.L., Allen, A.S. & Goldstein, D.B. Genic intolerance to functional variation and the interpretation of personal genomes. *PLoS Genet.* **9**, e1003709 (2013).
33. Georgi, B., Voight, B.F. & Bućan, M. From mouse to human: evolutionary genomics analysis of human orthologs of essential genes. *PLoS Genet.* **9**, e1003484 (2013).
34. Uddin, M. *et al.* Brain-expressed exons under purifying selection are enriched for *de novo* mutations in autism spectrum disorder. *Nat. Genet.* **46**, 742–747 (2014).
35. De Rubeis, S. *et al.* Synaptic, transcriptional and chromatin genes disrupted in autism. *Nature* **515**, 209–215 (2014).
36. Epi4K Consortium & Epilepsy Phenome/Genome Project. *De novo* mutations in epileptic encephalopathies. *Nature* **501**, 217–221 (2013).
37. Deciphering Developmental Disorders Study. Large-scale discovery of novel genetic causes of developmental disorders. *Nature* **519**, 223–228 (2015).
38. Hamdan, F.F. *et al. De novo* mutations in moderate or severe intellectual disability. *PLoS Genet.* **10**, e1004772 (2014).
39. Rauch, A. *et al.* Range of genetic mutations associated with severe non-syndromic sporadic intellectual disability: an exome sequencing study. *Lancet* **380**, 1674–1682 (2012).
40. de Ligt, J. *et al.* Diagnostic exome sequencing in persons with severe intellectual disability. *N. Engl. J. Med.* **367**, 1921–1929 (2012).
41. Ginsburg, D. & Bowie, E.J. Molecular genetics of von Willebrand disease. *Blood* **79**, 2507–2519 (1992).
42. Iossifov, I. *et al.* The contribution of *de novo* coding mutations to autism spectrum disorder. *Nature* **515**, 216–221 (2014).
43. Orosco, L.A. *et al.* Loss of *Wdfy3* in mice alters cerebral cortical neurogenesis reflecting aspects of the autism pathology. *Nat. Commun.* **5**, 4692 (2014).
44. Eyre-Walker, A. & Eyre-Walker, Y.C. How much of the variation in the mutation rate along the human genome can be explained? *G3 (Bethesda)* **4**, 1667–1670 (2014).
45. Kimura, M. & Ohta, T. On some principles governing molecular evolution. *Proc. Natl. Acad. Sci. USA* **71**, 2848–2852 (1974).
46. Ségurel, L., Wyman, M.J. & Przeworski, M. Determinants of mutation rate variation in the human germline. *Annu. Rev. Genomics Hum. Genet.* **15**, 47–70 (2014).
47. Hussin, J.G. *et al.* Recombination affects accumulation of damaging and disease-associated mutations in human populations. *Nat. Genet.* **47**, 400–404 (2015).
48. Koren, A. *et al.* Genetic variation in human DNA replication timing. *Cell* **159**, 1015–1026 (2014).
49. Siepel, A. & Haussler, D. Phylogenetic estimation of context-dependent substitution rates by maximum likelihood. *Mol. Biol. Evol.* **21**, 468–488 (2004).

ONLINE METHODS

Sourcing population samples. Samples were obtained from phase 1 of the 1000 Genomes Project. We considered only the variants from individuals of African, European and East Asian ancestry.

Selection of intergenic noncoding sequences. Intergenic sequences were defined as the full set of genomic sequences that are not annotated in Ensembl Biomart (version 75) and RefSeq Genes. We then removed centromeres, telomeres, repetitive regions and sequences not present in the accessibility mask (version 20120824) filter of the 1000 Genomes Project. Within these intergenic regions, we identified variants for the three populations for use in downstream analysis. More details are provided in the **Supplementary Note**.

Statistical framework to model substitution probabilities for intergenic noncoding regions. We initially describe a simple model that does not take into account local sequence context and then build upon this by incorporating additional local sequence contexts.

Suppose that we observe n_C occurrences of nucleotide C in the reference genome. A subset of these n_C sites will be polymorphic within the population of individuals. Let n_{CA} represent the number of sites where a C-to-A nucleotide change has occurred. Similarly, n_{CG} is the number of sites where a C-to-G change has occurred and n_{CT} is the number of sites where a C-to-T change has occurred. Then, the probability of nucleotide substitution or polymorphism within the population can be described using a multinomial distribution

$$\frac{n_C!}{(n_C - n_{CA} - n_{CG} - n_{CT})! n_{CA}! n_{CG} n_{CT}!} {\alpha_{CA}}^{n_{CA}} {\alpha_{CG}}^{n_{CG}} {\alpha_{CT}}^{n_{CT}} (1 - \alpha_{CA} - \alpha_{CG} - \alpha_{CT})^{(n_C - n_{CA} - n_{CG} - n_{CT})} \tag{1}$$

where the probabilities of observing a C-to-A, C-to-G or C-to-T substitution are expressed as α_{CA}, α_{CG} and α_{CT}, respectively. After iterating over all possible substitutions (A to C, A to G, A to T, C to A, C to G, C to T, T to A, T to G, T to C, G to A, G to C and G to T), we merge the reverse-complementary pairs (for example, A to C was merged with T to G, etc.) to yield six 'substitution classes' as parameters for the simple model, which we refer to as the 1-mer model. We then use maximum-likelihood estimation (MLE) to find the substitution probability estimates for all possible substitutions.

This model can be naturally extended to consider the effects of local sequence context by replacing the count of n_X occurrences of nucleotide X with the count of the occurrences of a particular nucleotide sequence context. For example, if we want to consider the local sequence context ACA, then we count the number of times the 3-mer sequence ACA occurs (n_{ACA}) in the reference genome. A subset of n_{ACA} sites will be polymorphic at the middle position C within a given population. Thus, let $n_{ACA \to AAA}$ represent the number of sites where a C-to-A nucleotide change has occurred at the middle position, $n_{ACA \to AGA}$ for C-to-G changes and $n_{ACA \to ATA}$ for C-to-T changes at the middle position. After iterating over all possible nucleotide combinations at the two ends (four possibilities at either side for a total of 16 possibilities) and substitutions at the middle position (three possible changes per nucleotide for a total of 12 possibilities), we merged the reverse-complementary pairs, yielding 96 substitution classes as parameters for the 3-mer model.

Analogously, we extended the size of the sequence context window to evaluate the 5-mer model and the 7-mer model by considering additional fixed nucleotides (two and three, respectively) on either side of the polymorphic site, thereby estimating a total of 1,536 parameters for the 5-mer model and 24,576 parameters for the 7-mer model. More details are provided in the **Supplementary Note**.

Log-likelihood ratio testing for model comparison. We initially find the likelihood of the observed distribution of polymorphic sites using the substitution rate parameters for a sequence context model. We then calculate the likelihood-ratio test statistic as

$$-2\ln\left(\mathrm{L}[\text{data} \mid \text{context } S_1]\right) + 2\ln\left(\mathrm{L}[\text{data} \mid \text{context } S_2]\right) \tag{2}$$

where S_1 and S_2 represent parameters estimated from two competing sequence context models. The test is χ^2 distributed, with the degrees of freedom equal to the difference in the number of parameters between the two models (for example, comparing the 3-mer model with the 1-mer model requires 90 degrees of freedom; comparing the 7-mer model with the 3-mer model requires 24,480 degrees of freedom).

Selection of HapMap variants. Single-nucleotide polymorphic variants were obtained from the phase 3 release of the HapMap Project. We considered only the variants from individuals of African ancestry present in our intergenic noncoding sequences. More details are provided in the **Supplementary Note**.

Incorporating prior information into the statistical framework. Because the likelihood of our framework is based on a multinomial distribution, we use its conjugate prior, that is, the dirichlet distribution, for different sequence context models. For inference in the intergenic noncoding genome, we select the objective version of the prior for our analysis, with all concentration parameters of the dirichlet prior set as 1. We then use the maximum a posteriori (MAP) estimates to find the substitution probability estimates for all possible substitutions. More details are provided in the **Supplementary Note**.

Bayes factor analysis for model comparison. We calculated the approximate posterior likelihood, using Chib's method, on the overall data using the MAP estimates of the substitution probabilities for a specific sequence context model found before. We then calculate the ABF as

$$\frac{\text{Posterior likelihood under model}_2}{\text{Posterior likelihood under model}_1} = \frac{\text{Prob}\left(\text{data}|\text{context}\,S_2\right) \times \text{Prob}\left(\text{context}\,S_2\right)}{\text{Prob}\left(\text{data}|\text{context}\,S_1\right) \times \text{Prob}\left(\text{context}\,S_1\right)} \tag{3}$$

where S_1 and S_2 represent parameters estimated from two competing sequence context models. We use the Jefferey's scale for interpreting the ABFs, where the ratio if greater than 100 is considered to be decisive evidence against model$_1$. More details are provided in the **Supplementary Note**.

Regression modeling and feature selection. We considered each substitution class separately and created an additional substitution class for each of the three possible changes within a CpG context, resulting in nine substitution classes. For each substitution class, we consider the initial regression model

$$\Pr[X_1 \to X_2|S] = \alpha + \beta_1 p_1^{\mathrm{C}} + \beta_2 p_1^{\mathrm{G}} + \beta_3 p_1^{\mathrm{T}} + \ldots + \beta_n p_7^{\mathrm{T}} + \varepsilon \tag{4}$$

where the probability that a nucleotide changes from X_1 to X_2 is modeled using a position-based variable p, a set of bases (for example, {C, G or T} where A is the reference base) denoted by the superscript for p, each position (= 1, 2, 3, 5, 6 or 7) denoted by the subscript for p within sequence context S, intercept α and error term ε. We assigned A as the reference nucleotide at each position and encoded the single nucleotide present at each position as the combination of three thermometer variables (for example, 0,0,0 = A; 0,0,1 = C; 0,1,0 = G; 1,0,0 = T). Next, we examined non-additivity (interactions) between nucleotides at sequence context positions. Rather than including all possible interaction terms, we employed feature selection (model training and testing to select the most informative features) and incorporated these terms into the final model. We considered two-way, three-way and four-way interactions across positions within the 7-mer as

$$\Pr[X_1 \rightarrow X_2|S] = \alpha + \beta_1 p_1^{C} + \beta_2 p_1^{G} + \beta_3 p_1^{T} + \ldots + \beta_n p_7^{T} + \quad (5)$$

$$\beta_a p_i^w \times p_j^x + \ldots + \beta_b p_i^w \times p_j^x \times p_k^y + \ldots + \beta_c p_i^w \times p_j^x \times p_k^y \times p_l^z + \ldots + \varepsilon$$

where the probability that a nucleotide changes from X_1 to X_2 is modeled as described in equation (4) and a set of additional terms related to interactions is also incorporated. The effect of the interaction is represented by term β_a for two-way interactions, β_b for three-way interactions and β_c for four-way interactions.

We then divided the genome into two distinct sets for feature selection, using all even-numbered chromosomes for training and all odd-numbered chromosomes for model testing. During training, we performed stepwise forward regression for each level of interaction of increasing complexity (first two-way, then three-way and finally four-way). For each level of interaction, we further trained the model by sequentially incorporating interaction terms, one at a time, and evaluating whether each term improved the model using the ANOVA *F* test. The most informative interaction term was added to the model at each step. For higher-order (three-way and four-way) interactions, we ensured that a proposed feature maintained the hierarchy constraint (a selected four-way term must bring with it all of its associated three-way and two-way terms), thereby adding degrees of freedom to our *F*-test assessment. We repeated this process until no additional features further improved the model (all proposed features had $P > 0.001$ by the *F* test). As our final model, we selected the trained model with the lowest mean-squared error, calculated via cross-validation within each substitution class. The 3-mer calculations considered all 2-way interactions plus single (positions 3 and 5 only) features. More details are provided in the **Supplementary Note**.

Sourcing CpG methylation data. We obtained CpG methylation data for our intergenic regions of interest from whole-genome bisulfite sequencing studies performed on germline[19] (sperm or oocyte), blastocyst, blood and brain[20] tissues. We performed our analysis on the 7,059,740 intergenic CpG sites that were methylated and the 651,479 intergenic CpG sites that were unmethylated in all three samples in the sperm tissue. We summarized the methylation signal across all samples for a tissue by calculating the mean intensity.

Sequence motif identification. We examined the top and bottom ten sequences for each substitution class and manually identified a total of six motifs that we tested in each substitution class, stratified by CpG context. This results in a total of (9 substitution classes) × (2 tails, high and low) × (6 motifs) = 108 tests. Note that we required nominal *P* value = 4.6×10^{-4} (Bonferroni correction for multiple testing). Testing was performed via Fisher's exact test. More details are provided in the **Supplementary Note**.

Recombination and substitution rates. We obtained a recombination rate map of the YRI (Yoruba) population from the phase 1 release of the 1000 Genomes Project and segregated our intergenic noncoding regions of interest into ones with high (>3 cM/Mb) and low (<0.05 cM/Mb) recombination rates. More details are provided in the **Supplementary Note**.

Human and primate divergence. We obtained human-chimpanzee and human-macaque chain and netted alignments from the Golden Path directories in the UCSC Genome Browser and found divergence between the human-primate pair by calculating fixed differences between the aligned intergenic noncoding sequences at each 7-mer sequence context. More details are provided in the **Supplementary Note**.

Variants across the frequency spectrum. We defined rare variants as those occurring fewer than two times in the population and low- and high-frequency variants as those with minor allele frequency (MAF) >1%. We only considered the intergenic noncoding variants present in the 1000 Genomes Project belonging to individuals of African ancestry and found 2,789,383 rare and 8,019,893 low- or high-frequency variants. More details are provided in the **Supplementary Note**.

***De novo* mutations.** We only considered the *de novo* mutations occurring in the accessible regions of the 1000 Genomes Project. For each motif class, we found the expected number of mutations under a normalized 1-mer sequence context model. More details are provided in the **Supplementary Note**.

Extension of the substitution probability framework in the coding region. To model substitution probabilities for the coding genome, we used the statistical model developed for intergenic regions with the following modifications. First, we accounted for codon position effects (a given sequence context around a polymorphic site may occur at three different positions on a codon), which can lead to amino acid changes that may be subject to different levels of selective constraint. Second, we used probabilities learned from the intergenic noncoding region model as our Bayesian prior for the coding model. The parameters for this dirichlet distribution prior include the weighted baseline probabilities from the intergenic noncoding region as shape parameters. More details are provided in the **Supplementary Note**.

Selection of coding sequences. We selected the exonic coordinates of the longest transcript for each gene annotated in Ensembl Biomart (version 75). We only considered transcripts where (i) the total exonic region length was a multiple of three and (ii) 90% or more of this length was present in the combined accessibility mask (version 20120824) filter of the 1000 Genomes Project. This yielded 16,386 autosomal transcripts and 679 transcripts from the X chromosome.

To test our model in a different data set, SNP sites for ~4,300 individuals of European ancestry were obtained from the Exome Variant Server (EVS; downloaded on 26 August 2013). For EVS data, to obtain a representative spectrum of allele frequencies (and the impact of background selection) observed from the smaller set of individuals found in the 1000 Genomes Project data, we only considered variants with a frequency greater than 0.03%. More details are provided in the **Supplementary Note**.

Annotation of SNP variants in the autosomal coding genome. For both 1000 Genomes Project and EVS data, we manually annotated the type of codon change caused by each variant specific to the transcript.

Scaling the substitution probability estimates for a larger sample. To calibrate our model (built using the 1000 Genomes Project data set) for use with the larger EVS data set, we rescaled the substitution probabilities estimated using the 1000 Genomes Project data to make them proportional to the EVS data set. We used a constant scaling factor defined as

$$\frac{\text{Overall substitution probability in the new data set}}{\text{Overall substitution probability in the 1000 Genomes data set}} \quad (7)$$

on all substitution probabilities in the new data set.

Simulating variability in substitution probabilities within amino acid replacement classes. We start by randomly distributing the observed substitutions within the amino acid replacement class, using a fixed-rate model. We then calculate the respective 7-mer probabilities from the randomized data set using our multinomial distribution model for randomization and then find the variance in the new substitution probability estimates for that class. We use 1 million simulations to generate the distribution of substitution probabilities.

Measuring the effects of selection on polymorphisms in the coding region. To minimize the effects of selection on initial estimates of substitution probabilities, we selected intergenic noncoding intervals for model development. Assuming that the mechanisms that introduce new mutations into coding regions are similar to those at work in the noncoding genome, we infer that the relative ratio of coding to noncoding substitution probabilities could indicate natural selection occurring in the coding genome. To quantify the effect of selection on substitution probabilities, we measured the $\log_{10}$ ratio of coding to noncoding substitution probabilities using all coding variants observed in the 1000 Genomes Project African group. More details are provided in the **Supplementary Note**.

doi:10.1038/ng.3511

Calculating tolerance scores for genes. We find the expected distribution of polymorphism levels for each gene by performing simulations from the standard multinomial distribution using our coding substitution probability estimates. We then normalize the difference between the observed levels of polymorphism and those generated from simulations, to obtain the gene tolerance score defined as

$$\frac{(\mu_{\mathrm{NS}} - n_{\mathrm{NS}})}{\sigma_{\mathrm{NS}}} \tag{8}$$

where μ_{NS} and σ_{NS} represent the mean and standard deviation of nonsynonymous polymorphisms generated from simulations based on our model and n_{NS} is the empirical number of nonsynonymous polymorphism observed in the data. A positive gene score indicates that the number of observed substitutions is fewer than expected and identifies genes experiencing stronger than average purifying selection.

Categorizing genes on the basis of tolerance scores. We subdivided genes into various categories, that is, essential genes (where knockout of the mouse homolog is lethal), ubiquitously expressed genes, genes with known phenotypes described in OMIM, immune-related genes, keratin genes and olfactory genes. The data set from ref. 33 was used to find the first two categories, and ref. 32 was used to classify genes in OMIM. OMIM subcategorizes genes according to mutational models, including *de novo*, dominant, haploinsufficient or recessive. In our analysis, we merged OMIM's *de novo*, dominant and haploinsufficient categories, treating them as a single category. We used the DAVID ontology database (version 6.7) to classify immune-related, keratin and olfactory genes. We considered the gene lists published in the latest *de novo* sequencing analysis reports on autism[35], epilepsy[36], intellectual disability[38–40] and developmental disorder[37] as the gene sets belonging to these diseases. We merged the gene lists of the aforementioned diseases, treating them as a single category belonging to 'all neuropsychiatric disease'.

AUC comparison between competing gene scores on different gene sets. We used the receiver operating characteristic (ROC) curve to compare the performance of our gene scores against previously annotated scores for classifying genes into the gene sets we described above. We fitted a linear classifier using the three different gene scores on each gene set and found the area under the curve (AUC) for each. More details are provided in the **Supplementary Note**.

Calculating tolerance scores for amino acids. We find the expected distribution of polymorphism levels for a specific amino acid encoded by a gene by performing simulations from the standard multinomial distribution using our coding substitution probability estimates. For a given gene, we then normalize the difference between the observed numbers of changes at a specific amino acid versus the number of changes expected from simulation using the equation

$$\frac{(\mu_{\mathrm{AA}} - n_{\mathrm{AA}})}{\sigma_{\mathrm{AA}}} \tag{9}$$

where μ_{AA} and σ_{AA} represent the mean and standard deviation of the specific amino acid replacement polymorphisms generated from simulations based on our model and n_{AA} is the empirical number of amino acid replacement polymorphisms observed in the data. We consider the normalized value in equation (9) as the final tolerance score for that amino acid within the given gene. We interpret a positive amino acid tolerance score to indicate that the observed number of changes for that specific amino acid for the given gene was even fewer than expected. Thus, the amino acid tolerance score serves to identify amino acids experiencing stronger than average purifying selection.

Sourcing information about pathogenic variants. We used the HGMD (professional 2014.4) to identify pathogenic variants for our autosomal genes of interest, which supplied 60,504 variants distributed over 3,647 genes for 5,359 putative human disorders.

Application of gene and amino acid score on autism spectrum *de novo* sequencing data. We used the *de novo* sequencing data for autism spectrum disorder[42] to test the efficacy of our gene and amino acid score approach in identifying and prioritizing genes and variants newly associated with autism. We found the *de novo* mutations belonging to cases and controls separately for each of our genic sequences of interest and considered a total of 2,171 mutations in 2,508 cases and 1,421 mutations in 1,911 controls. For a uniform comparison of gene scores across different approaches[12,32], we only considered the top 752 intolerant genes identified from each approach. We chose 752 genes because this was the number of intolerant genes identified in ref. 12, which mapped to our autosomal genic sequences of interest (which pass the stringent criteria of sequencing quality in the 1000 Genomes Project). We used the odds ratio to find the burden of *de novo* mutations in cases as opposed to controls in the set of intolerant genes. Fisher's exact test was used to compare the significance of burden. For amino acid score, all statistical comparisons were performed using the Wilcoxon rank-sum test. More details are provided in the **Supplementary Note**.

Code availability. The computational pipelines used for probability estimation for the noncoding and coding genomes and for forward regression and feature selection are available upon request.

doi:10.1038/ng.3511